PAPER

Check for updates

Tailored mechanical properties of soybean oil-based non-isocyanate polyurethanes by copolymer integration†

Byeongju Jeon, [ID] [a] Kyoungmun Lee, [ID] [a] Jihoon Shin [ID] *[b,c] and Siyoung Q. Choi [ID] *[a]

Stiff thermoset polyurethane (PU) plays a crucial role in high-performance applications, particularly in industries requiring exceptional mechanical integrity, chemical resistance, and thermal stability. To reduce the environmental impact of PU production, (i) soybean oil has emerged as a renewable and abundant alternative to petroleum-based feedstocks, offering biodegradability and a reduced carbon footprint, while (ii) non-isocyanate polyurethane (NIPU) provides a greener approach by eliminating hazardous isocyanate compounds and avoiding isocyanate-functionalized chemicals. However, the development of soybean oil-based NIPU faces challenges in achieving the desired stiffness and resistance against fracture due to the large molecular size and inconsistent structure of soybean oil, which result in low crosslinking density and a lack of short-range ordering. To address the limitations of soybean oil-based NIPU, we developed a method that restricts polymer network relaxation by incorporating short-range ordered polymer segments using a copolymer with ethyl methacrylate (EMA) segments. Surpassing the highest mechanical properties reported for soybean oil-based NIPU to date, co-NIPU-*x* derived from copolymers with higher EMA content exhibits improved mechanical properties, demonstrating a four-fold increase in Young's modulus and a two-fold increase in tensile stress. The adjustable poly(2-aminoethylmethacrylate-*ran*-ethylmethacryate) (poly(AEMA-*ran*-EMA)) composition ratio allows for a wide range of mechanical properties, with Young's modulus ranging from 60 to 1030 MPa and tensile stress from 2.1 to 25 MPa. Furthermore, these NIPU samples exhibited enhanced adhesion properties with lap shear strength exceeding 7 MPa, significantly higher than those of traditional formulations. The thermal stability was improved with the NIPU samples resisting structural degradation, and chemical resistance was confirmed by sufficient swelling ratios in both hydrophilic and hydrophobic solvents, underscoring their suitability for a broader range of industrial applications.

Green foundation

1. For the first time, we demonstrate that soybean oil—one of the most widely produced vegetable oils globally—can serve as a foundation for high-performance materials. Our innovative NIPU synthesis and formulation technology paves the way for advancing renewable bio-based polymers on a broader scale.

2. This work addresses the longstanding challenge of weak mechanical properties in soybean oil-based non-isocyanate polyurethanes (NIPUs), leveraging its abundant and renewable nature to develop a novel NIPU with significantly enhanced and tunable mechanical performance with a Young's modulus up to 1030 MPa and a tensile strength of 25 MPa. Our NIPU formulation also exhibit enhanced adhesion properties, chemical resistance, and thermal stability.

3. We aim to optimize reactivity by refining the monomers used in polymer construction, significantly reducing reaction times. Furthermore, we plan to innovate adhesive formulations by substituting existing solvents, the only "non-green" component in our system, with highly volatile and eco-friendly alternatives that prioritize both human safety and environmental sustainability.

[a]Department of Chemical & Biomolecular Engineering, Korea Advanced Institute of Science and Technology (KAIST), 291 Daehak-ro, Yuseong-gu, Daejeon, 34141, Korea
[b]Center for CO2 & Energy, Korea Research Institute of Chemical Technology (KRICT), 141 Gajeong-ro, Yuseong-gu, Daejeon, 34114, Korea

[c]Department of Advanced Materials & Chemical Engineering, University of Science & Technology (UST), 217 Gajeong-ro, Yuseong-gu, Daejeon, 34113, Korea
†Electronic supplementary information (ESI) available. See DOI: https://doi.org/10.1039/d5gc00058k

Introduction

Polyurethane (PU) is a versatile polymer widely utilized across various industrial applications due to its tunable mechanical properties, chemical resistance, and thermal stability. Among different PU types, stiff thermosetting PU is particularly valuable in applications requiring high load-bearing capacity. In particular, it is essential in the automotive, aerospace, and construction industries,[1–4] where it enables strong interfacial bonding and high mechanical integrity. Additionally, PU-based thermosets exhibit excellent resistance to chemicals and temperature fluctuations with the appropriate selection of chemical structures,[5,6] making them suitable for demanding industrial environments such as manufacturing, infrastructure maintenance, and high-performance assemblies. Beyond adhesives, rigid PU can be widely used in stiffer variants ideal for applications requiring high load-bearing capacity, such as rigid foams and coatings.[7–10]

Among the various precursors for synthesizing NIPU, soybean oil has garnered considerable attention for its renewable and abundant supply, as well as its environmental sustainability. This feedstock can be transformed into epoxidized soybean oil (ESBO), which is subsequently converted using carbon dioxide to produce carbonated soybean oil (CSBO) rich in 5CC functional groups.[11,12] Soybean oil, which exceeded 398 million metric tons in global production in 2023/24,[13] is one of the most produced vegetable oils worldwide, comparable to the total global production of plastics (380 million metric tons in 2018[14]). Its abundance ensures that the relatively small amount of soybean oil required for NIPU production (polyurethane accounting for ~5% of all polymers[15]) poses little threat to the global food supply or to the affordability of soybean oil. Substituting petroleum-based feedstocks with soybean-based alternatives addresses concerns related to fossil fuel depletion, global warming, smog formation, and ecological toxicity.[16]

To further enhance the environmental benefits of soybean oil-based polyurethane materials, non-isocyanate polyurethane (NIPU) has emerged as a promising alternative to conventional polyurethane due to its differentiated synthesis method. While typical isocyanate polyurethane (IPU) is synthesized by reacting isocyanate-functionalized chemicals, which pose significant health and environmental risks,[17,18] NIPU synthesis employs chemical reactions that form carbamate linkages without the need for isocyanate compounds, including the reaction of a 5-membered cyclic carbonate (5CC) group with a diamine.[19] In addition to posing minimal health and environmental concerns during its production and use, NIPU exhibits unique characteristics including extra primary and secondary hydroxyl groups at the β-carbon atom adjacent to the carbamate groups. A molecular structure of this nature is referred to as polyhydroxyurethane (PHU). This differentiates NIPU from conventional polyurethanes, endowing it with enhanced adhesion, chemical resistance, and thermal stability.[20–22] By leveraging these advantages, NIPU can be readily applied in practical scenarios, as its properties can be freely adjusted to meet specific requirements.[23–25]

Numerous studies have explored the utilization of soybean oil-based NIPU, including the development of fully bio-based NIPU using amine groups as renewable reactants,[26–28] the addition of azetidinium groups that impart antibacterial properties to NIPU,[29] and the development of reprocessable NIPU through the transcarbomylation reaction.[30–32] However, despite its promising outlook, soy-based NIPU faces challenges due to its inherent softness and low load-bearing capacity, limiting its applicability in certain high-strength application scenarios. Previous research efforts have predominantly yielded NIPU formulations with soft characteristics, failing to achieve the properties comparable to those of conventional polyurethanes. The highest reported Young's modulus for NIPU to date is 224 MPa, with a tensile strength of 15 MPa.[27] These values are significantly lower than those achievable with isocyanate polyurethane[33] or NIPU without using soybean oil,[9,34,35] which can reach the ~GPa unit scale for Young's modulus. The inclusion of soybean oil in NIPU generally results in a glass transition temperature similar to or lower than ambient temperature,[34,36,37] indicating unrestricted rotational motion of the segments constituting the cross-linked network. Unlike typical petroleum-based refined compounds or repetitive polymers, triglycerides lack regularity in their molecular arrangement due to variations in the combination of attached fatty acids among different molecules. This structural variability impedes the close proximity required for effective intermolecular attraction, thereby limiting the stiffness.[38] Therefore, there is a need to overcome these limitations by developing a novel synthesis method for soybean oil-based NIPU that retains the superior properties of NIPU while simultaneously enhancing mechanical properties, ultimately enabling the use of soybean oil in versatile applications.

As previously mentioned, the properties of NIPU can be influenced by the type of amine-terminated reactant interacting with CSBO, which determines the mobility of the segments.[27,34] Additionally, to maintain the superior adhesion and chemical/thermal stability properties of NIPU mentioned earlier, it is essential to form a sufficient amount of carbamate groups. Based on this understanding, we have deliberately chosen substances capable of reacting with CSBO while also possessing a consistent structure to address the intrinsic softness of soybean-based non-isocyanate polyurethane (NIPU). Here, we adopt copolymerization to promote molecular organization within the polymer matrix, thereby enhancing mechanical properties. By repetitively incorporating identical monomers that can be linked with CSBO, we aim to induce close proximity. Studies have shown that certain polymers exhibit short-range order or so-called "local order", as exemplified by the *n*-alkyl acrylate polymer and the cycloalkyl methacrylate polymer with consistent intersegmental arrangement at a scale larger than simple atomic contact.[39] Furthermore, the formation of spatially restricted layer structures, demonstrated in studies on polymers like amorphous poly(ethylmethacrylate) (PEMA), underscores the potential for tailored molecular arrangements to influence material properties.[40]

Considering these criteria, we have deliberately selected two specific monomers for random copolymerization: 2-aminoethyl methacrylate (AEMA) and ethyl methacrylate (EMA). By adjusting the length of EMA segments in the copolymer, our study aims to control the mechanical properties of the resulting soybean oil-based NIPU formulations, thus expanding the applicability of these materials in various industrial settings.

Experimental section

Materials

Nitrogen (>99.9%) and carbon dioxide (>99.9%) were purchased from Samospgas. VA-044 (>97.0%) was purchased from FUJIFILM Wako Chemicals as an initiator. 2-Aminoethyl methacrylate hydrochloride (AEMA, contains 500 ppm phenothiazine as a stabilizer, 90%), ethyl methacrylate (EMA, 99%), tetrabutylammonium chloride (TBAC, ≥97.0%), decane (≥95.0%), ethyl acetate (99.8%), sodium hydroxide (98%, pellets, anhydrous), methanol (99.8%, anhydrous), deuterium oxide (99.9 atom % D), and chloroform-d (99.8 atom % D, contains 1% (v/v) TMS) were all purchased from Sigma-Aldrich. Dimethyl sulfoxide (DMSO, 99.0%) was purchased from JUNSEI. Ultrapure water was produced using a Millipore ICW-3000 purification system (>18 MΩ).

S,S'-Bis(α,α'-dimethyl-α''-acetic acid)trithiocarbonate was synthesized using a previously reported methodology.[41] The product was obtained as a yellowish powder.‡

Epoxidized soybean oil (ESBO) with an epoxy oxygen content of 4.2 mol per triglyceride was synthesized using a previously reported methodology.§[42]

CSBO preparation

The reaction was conducted in a closed-system batch reactor using a 15 mL glass vial sealed with a rubber septum. A mixture of 4 mL of epoxidized soybean oil (ESBO), 4 mL of decane, and 0.4 g of tetrabutylammonium chloride (TBAC) was added to the vial, and carbon dioxide (CO_2) gas was continuously bubbled through the reaction mixture for 2 days at 120 °C to facilitate carbonation. The CO_2 was introduced through a needle inserted into the septum, ensuring a steady gas flow. After the reaction, 20 mL of ethyl acetate was added to the crude product; the TBAC was extracted three times using a separatory funnel and 20 mL of ultrapure water. The residual solution was heated at 100 °C to produce a brownish, viscous substance.¶

Copolymer preparation

The RAFT copolymerization of AEMA and EMA proceeded as follows. 0.75 mmol of AEMA, 6.75 mmol of EMA (molar ratio of AEMA to EMA is 1 : 9), 9.38 µmol of S,S'-bis(α,α'-dimethyl-α''-acetic acid)trithiocarbonate (RAFT agent), and 3.75 µmol of VA-044 (initiator) were dissolved in methanol to produce a 15 mL solution in a 50 mL vial. Nitrogen gas was purged for 10 minutes and then sealed, in order to remove atmospheric oxygen. The polymerization reaction was conducted at 65 °C for 24 hours, with stirring at 600 rpm. The reaction was quenched by rapidly cooling the solution in an ice bath. After dissolving an equal quantity (in moles) of sodium hydroxide into the solution relative to the initial amount of AEMA, the mixture was stirred for an hour in order to convert the amine salt pendant group into a primary amine. Purification was performed twice using a dialysis sack against 1 L of ultrapure water. In order to generate copolymers with different compositions, the total number of moles of AEMA and EMA reactants was set to 7.5 mmol and the previous process was repeated while varying the molar ratios to 3 : 17, 9 : 31, 3 : 7, and 1 : 1. Accordingly, the copolymers are labeled as "10A90E", "15A85E", "22A78E", "30A70E", and "50A50E", respectively.

Copolymer characterization

^{1}H NMR spectroscopy (Bruker 400 MHz, Bruker), differential scanning calorimetry (DSC 214, Polyma), and thermogravimetric analysis (TG209 F1 Libra, NETZSCH) were conducted for copolymer characterization. Molecular weight analysis was conducted using size exclusion chromatography (EcoSEC HLC-8320 GPC, Tosoh), employing a polystyrene column as the standard material and tetrahydrofuran + 1 wt% DEA as the mobile phase. PAEMA was also synthesized using an identical procedure without any EMA input.

Co-NIPU-x synthesis

The synthesized poly(2-aminoethylmethacrylate-ran-ethylmethacryate) (poly(AEMA-ran-EMA)) and CSBO were mixed with 20 mL of dimethyl sulfoxide (DMSO). Each reactant was prepared with a 1 : 1 stoichiometric ratio of the primary amine group of poly(AEMA-ran-EMA) to the 5-cyclic carbonate group of CSBO. The total mass of reagents was set to 0.50 g. The mixture was heated at 120 °C for 10 minutes to completely dissolve the reactants in DMSO. The solution was then placed into a 4 cm × 4 cm × 2 cm square Teflon dish (HANTECH) and reacted at 120 °C for 24 hours. For curing, the product was heated at 135 °C for 6 hours. The NIPU samples synthesized from "10A90E", "15A85E", "22A78E', "30A70E", and "50A50E"

---

‡ S,S'-Bis(α,α'-dimethyl-α''-acetic acid)trithiocarbonate characterization. ^{1}H NMR (400 MHz, CDCl$_3$): δ = 1.72 (12H, 1-CH$_3$) ppm (Fig. S1†). ^{13}C NMR (400 MHz, CDCl$_3$): δ = 25.17 (1-CH$_3$), 55.83 (2-C), 179.99 (3-COO), and 217.23 (4-CS$_3$) ppm (Fig. S2†).

§ Epoxidized soybean oil (ESBO) characterization. ^{1}H NMR (400 MHz, CDCl$_3$): δ = 1.24–1.37 (m, 7-CH$_2$, 8-CH$_3$), 1.42–1.82 (m, 4-CH$_2$ next to epoxide, 6-CH$_2$), 1.42–1.82 (5-COOCH$_2$), 2.86–3.17 (m, 8.5H, 3-CH in epoxide), 4.11–4.30 (m, 4H, 2-CH$_2$), and 5.25 (m, 1H, 1-CH) ppm (Fig. S7a†). FTIR (ATR): $\tilde{v}_{max}$ = 2854, 2926 (C–H), 1736 (C=O, ester), 1387, 1457 (C–C), 1149, and 1247 (C–O) cm^{-1} (Fig. S3a†).

¶ Carbonated soybean oil (CSBO) characterization. ^{1}H NMR (400 MHz, CDCl$_3$): δ = 1.26–1.40 (m, 7-CH$_2$, 8-CH$_3$), 1.46–1.72 (m, 4-CH$_2$ next to epoxide, 5-COOCH$_2$, 6-CH$_2$), 2.06–2.39 (m, 4-CH$_2$ next to epoxide, 5-COOCH$_2$, 6-CH$_2$, 10-CH$_2$ next to cyclic carbonate), 2.91 (m, 3-CH in epoxide), 4.11–4.33 (m, 4H, 2-CH$_2$), 4.58–5.15 (m, 1-CH in cyclic carbonate), 5.28 (m, 1-CH), and 5.72–5.99 (m, 9-CH in cyclic carbonate) ppm (Fig. S7b†). FTIR (ATR): $\tilde{v}_{max}$ = 2854, 2924 (C–H), 1802 (C=O, cyclic carbonate), 1736 (C=O, ester), 1259, 1365, 1391, 1464 (C–C), and 1175 (C–O) (Fig. S3b†).

were respectively labeled as "co-NIPU-1", "co-NIPU-2", "co-NIPU-3", "co-NIPU-4", and "co-NIPU-5". The same method was used to react CSBO with poly-(2-aminoethyl methacrylate) (PAEMA). The polymer containing amine pendant groups and CSBO containing 5CC groups were mixed at different stoichiometric ratios of 1 : 0.25, 1 : 0.375, 1 : 0.5, 1 : 0.625, 1 : 0.75, and 1 : 1.

Spectroscopic characterization of Co-NIPU-x

Fourier transform infrared spectra were obtained in ATR mode using an Alpha-P spectrometer (Bruker). The spectral data were collected from 4000 cm^{-1} to 400 cm^{-1} with a nominal resolution of 2 cm^{-1}. For the co-NIPU-1 sample, the spectra were recorded with a nominal resolution of 1 cm^{-1} to enhance spectral details.

Mechanical, thermal, and physicochemical characterization of Co-NIPU-x

Stress–strain curve measurements of the co-NIPU-x series were performed on NIPU samples with a rectangular (30 mm × 3 mm) shape at ambient temperature (25 °C). All sample thicknesses were smaller than 0.5 mm. The apparatus was a custom-made universal tensile machine with a 200 N load cell (DBCM-20, BONSHIN). The software controlled the speed of the motor (RKE543AC, Oriental Motor) to 1 mm min^{-1}. All co-NIPU-x series were analyzed 2–4 times to obtain Young's modulus (E), ultimate tensile strength (σ_R), and elongation at break (ε_R). A low-temperature high-resolution powder X-ray diffractometer (SmartLab, RIGAKU) with a Cu K-alpha I source was used to detect the short-range order of each co-NIPU-x sample. The sample was prepared in the form of a powder by grinding with a mortar. The 2θ range was set from 2° to 30°. Low-temperature differential scanning calorimetry (DSC 214 Polyma, NETZSCH) was also conducted for each co-NIPU-x sample at a heating rate of 20 °C min^{-1} under a nitrogen atmosphere. Each sample was heated from −50 °C to 150 °C. In order to clearly identify broad peaks (or halos), a smoothing process (adjacent averaging method, 20 pts) was applied.

To measure the adhesion properties of co-NIPU-x samples, a lap shear test was conducted using a soda-lime glass substrate. The synthesis method for co-NIPU-x remained the same, except that the reaction was conducted in a 15 mL vial instead of a Teflon dish, and the solvent DMSO was evaporated until the solution volume was reduced to 1.5 mL to form a gel. The swollen product was subsequently spread onto soda-lime glass and subjected to a pressure of 20 kPa using a weight, allowing the reaction to proceed under consistent temperature conditions (120 °C). The scale of the lap shear test samples was determined as shown in Fig. S4.† The total reaction time was set to 24 hours, followed by curing at 125 °C for 6 hours. The samples were tested for lap shear strength using a universal tensile machine at a pulling speed of 1 mm min^{-1}, with each test repeated 2–3 times. In addition, to verify the practical load-bearing capacity, samples were prepared using the same method as before on a 6.8 cm^2 area of the same type of sub-

strate. A weight is placed 1.5 cm away from the support point to determine the threshold load-bearing capacity.

In order to determine the solvent resistance of the co-NIPU-x series, 10 mg of each NIPU sample was soaked in 10 mL of toluene and water for 48 hours and then dried in a vacuum oven at 70 °C for 3 hours in order to obtain the gel fraction and swelling ratio of each synthesized NIPU sample. To evaluate the thermal degradation behaviour of co-NIPU-x, thermogravimetric analysis (TG209 F1 Libra, NETZSCH) was performed under a nitrogen atmosphere. ∼10 mg of each sample was continuously heated in the range from 30 °C to 700 °C, at a heating rate of 10 °C min^{-1} (Scheme 1).

Results

Synthesis of poly(AEMA-ran-EMA)

To systematically determine the most suitable monomer for this study, we considered two main essential factors: (i) chemical compatibility to avoid undesired side reactions and (ii) balanced reactivity to ensure uniform copolymer composition. Among acrylate-based monomers, hydroxyl (–OH) or other reactive heteroatom-containing reactants except primary amines would introduce unintended reactivity. Furthermore, copolymers synthesized with monomers of significantly different reactivity ratios tend to exhibit non-uniform monomer incorporation, resulting in compositional drift along the polymer chain. For example, in the case of styrene and methacrylate monomers, the higher reactivity ratio of styrene ($r_{styrene}$) relative to methacrylate ($r_{methacrylate}$) leads to preferential incorporation of styrene in the early stages of living polymerization, followed by methacrylate polymerization at later stages.[43] This issue is avoided for reasons elaborated in the next two paragraphs. To circumvent this issue, 2-aminoethyl methacrylate (AEMA) and ethyl methacrylate (EMA) were chosen due to their similar backbone structures, ensuring a cleaner and more controlled polymerization process.

The selection of a homopolymer, block copolymer, or random copolymer as a reaction system was carefully made. Prior research suggests that the presence of 5-cyclic carbonate (5CC) groups in the polymer, enabling the formation of carbamate linkages, may lead to diminished conversion values when employing a 1 : 1 stoichiometric ratio between primary amine groups and 5CC groups.[44] To explore the potential occurrence of analogous challenges with homopolymers, the reaction between poly(2-aminoethyl methacrylate) (PAEMA) and carbonated soybean oil (CSBO) was conducted under controlled conditions at a fixed temperature (125 °C) and duration (48 hours). The molar ratio between the primary amine groups in PAEMA and the 5CC groups in CSBO was altered. The IR spectrum (Fig. S5†) confirmed a discernible emergence of the unreacted 5CC peak [a] and a subsequent decline in conversion efficiency below 100% when the molar quantity of 5CC groups surpasses one-fourth of the molar quantity of amine groups. Based on these findings, our research group postulated that the observed challenge in achieving optimal conver-

Scheme 1 Process overview: synthesis route of co-NIPU-x from CSBO, and their molecular structure/properties.

sion rates stems from the hindered accessibility of the two reaction sites—the 5CC group in CSBO and the amine pendant group in the polymer—due to steric hindrance.

We conducted calculations to determine the reactivity ratios of AEMA and EMA (Fig. 1). The RAFT polymerization method was used with a fixed 1 : 1 feed molar ratio of AEMA and EMA.
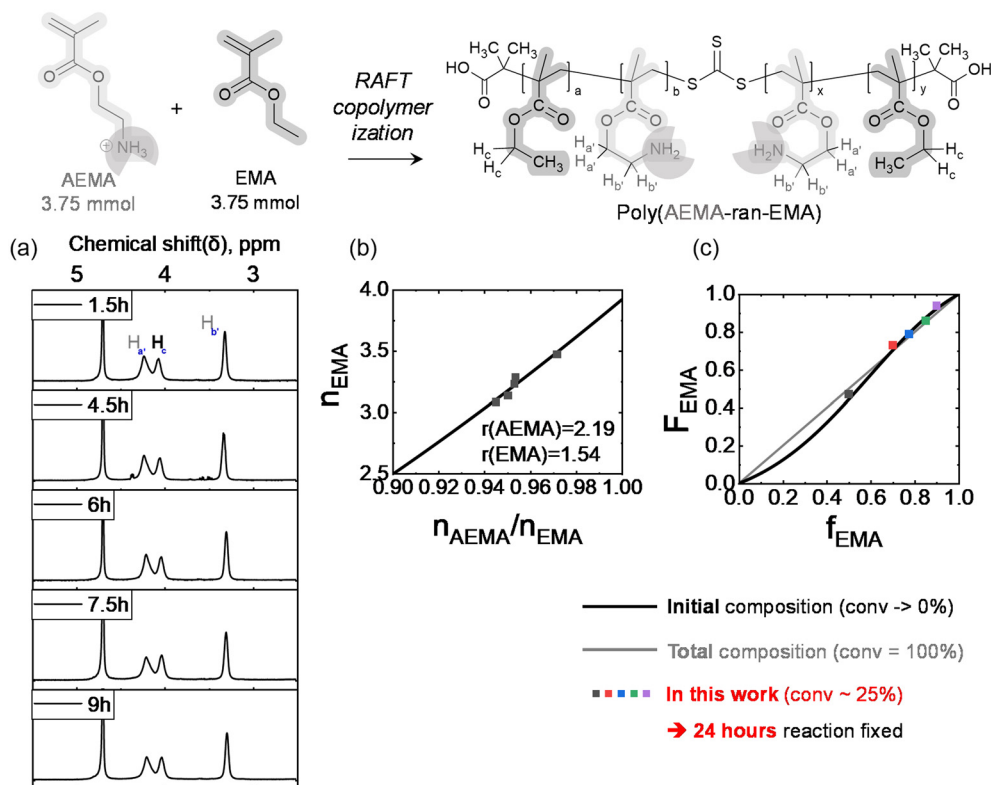
Fig. 1 Reactivity ratio analysis using the copolymer polymerization terminal model. (a) ^1H NMR (400 MHz, D_2O) of poly(AEMA-*ran*-EMA) in the case of f_{EMA} = 0.5, with varying reaction times: 1.5, 4.5, 6, 7.5, and 9 hours. (b) Copolymer polymerization terminal model fitting results and reactivity ratio values. (c) Plot showing the relationship between the initial feed ratio (f_{EMA}) and the mole ratio in the copolymer (F_{EMA}), as determined by the Mayo–Lewis equation (initial composition, black), the plot of $f_{EMA} = F_{EMA}$ (total composition, grey), and the experimental result (denoted by square markers).

The polymer products formed over time were extracted and analysed *via* ^1H NMR spectroscopy to determine the molar quantity of unreacted monomers, n_{AEMA} and n_{EMA} (Fig. 1a). The derived reactivity ratio (r_{EMA} = 1.54 < r_{AEMA} = 2.19) was then determined using a terminal model analysis[45] (Fig. 1b). The higher reactivity ratio of AEMA than that of EMA indicates that (i) AEMA exhibits greater reactivity than EMA and (ii) AEMA undergoes polymerization to a greater extent initially, leading to the formation of a polymer with a gradient structure[46] (Fig. 1b). Although the monomer selection was based on the rationale described earlier to minimize the impact of reactivity differences, the presence of the amine functional group remains a variable that cannot be eliminated, meaning the reactivity difference cannot be entirely negligible. To ensure a uniform ratio of the EMA component along the copolymer strand, the monomer ratio in the initial feed should closely match the monomer ratio in the final polymer. Therefore, all copolymer series for NIPU sample production are synthesized by adjusting the reaction time to 24 hours to target a conversion value of 25%. It was observed that the molar composition ratio (F_{AEMA}, F_{EMA}) of the synthesized copolymer closely approximated the theoretical value calculated using the Mayo–Lewis model, rather than the initial feed ratio (f_{AEMA}, f_{EMA}) (Fig. 1c). Based on the findings, the reaction time was adjusted

to 24 hours to maximize the uniformity of monomer distribution, thereby minimizing the compositional ratio disparity at both ends of the polymer strand (Table 1).

Taking into account the reaction time and conversion, we synthesized a series of poly(2-aminoethylmethacrylate-*ran*-ethylmethacrylate) (poly(AEMA-*ran*-EMA)) *via* reversible addition–fragmentation chain transfer (RAFT) copolymerization. The monomer, RAFT agent, and initiator were added in a molar ratio of 4000 : 5 : 2, respectively. In order to construct a series by varying the ratio of the two monomers constituting the copolymer, the feed molar ratios of EMA were set at 90, 85, 77.5, 70, and 50%. Considering the decomposition temperature of the initiator 2,2-azobis(2-methylpropionitrile) (AIBN) (65 to 80 °C) and the boiling point of the solvent methanol under atmospheric conditions, the reaction temperature was set at 65 °C.

The synthesized poly(AEMA-*ran*-EMA) ("10A90E", "15A85E", "22A78E", "30A70E", and "50A50E") were then characterized by ^1H NMR (Fig. 2). In the copolymer featuring protonated amine groups, the peak at δ = 4.3 ppm ($H_{a'}$) and the peak at δ = 3.3 ppm ($H_{b'}$) correspond to the AEMA component within the copolymer, while the peak at δ = 4.1 ppm (H_c) corresponds to the EMA component. It is important to note that the polymerized product contains NH_3^+ ions as pendant groups, requiring

Table 1 Synthetic conditions and properties of poly(AEMA-*ran*-EMA) series

| Copolymer	10A90E	15A85E	22A78E	30A70E	50A50E
f_{EMA} [a]	0.900	0.850	0.775	0.700	0.500
f_{AEMA} [b]	0.100	0.150	0.225	0.300	0.500
$F_{EMA,exp}$ [c]	0.940.	0.86	0.79	0.73	0.46
$F_{AEMA,exp}$ [d]	0.060	0.14	0.21	0.27	0.54
$F_{EMA,initial}$ [e]	0.923	0.875	0.794	0.703	0.443
$M_{n,target}$ (kg mol^{-1})	23.1	23.3	23.5	23.7	24.3
Conversion	0.22	0.22	0.25	0.26	0.22
$M_{n,SEC}$ [f] (kg mol^{-1}) ($Đ$)	44 (2.1)	39 (1.9)	52 (1.8)	42 (1.7)	17 (1.4)
$T_{10\%,TGA}$ [g] (°C)	272.0	268.0	265.8	202.6	218.6
$T_{g,DSC}$ [h] (°C)	66	70	67	64	61

[a] Initial feed of EMA. [b] Initial feed of AEMA. [c] Molar component of EMA in the copolymer, experimental value determined by ^{1}H NMR spectroscopy (400 MHz, D$_2$O). [d] Molar component of AEMA in the copolymer, experimental value determined by ^{1}H NMR spectroscopy (400 MHz, D$_2$O). [e] Molar component of EMA in the copolymer, theoretical value calculated using the Mayo–Lewis equation. [f] Molar weight of co-(AEMA-*ran*-EMA) detected by size exclusion chromatography. See Fig. S6† for detailed results. [g] Temperature corresponding to 10% thermal decomposition, derived from derivative thermogravimetric analysis (DTG). [h] Glass transition temperature determined by differential scanning calorimetry (DSC).

the addition of an equivalent amount of a base to synthesize the final precursor. Two main peaks corresponding to the AEMA pendant group exhibit upfield shifts after the addition of a base: δ = 4.3 ppm (H$_{a'}$) shifts to δ = 4.1 ppm (H$_a$) and δ = 3.3 ppm (H$_{b'}$) shifts to δ = 3.0 ppm (H$_b$). This result indicates that the protonated amine groups (–NH$_{3+}$) in the polymer were deprotonated to form neutral amine (–NH$_2$) groups upon base addition.[47]

The overall molecular study, including ^{1}H NMR (Fig. 1), size exclusion chromatography (SEC), differential scanning calorimetry (DSC), and thermogravimetric analysis (TGA), is summarized in Table 1. All copolymers except 50A50E exceeded the target molecular weight (Fig. S6†). The deviation from the target molecular weight appears to be due to the incomplete reaction of the RAFT agent employed during the synthesis. Additionally, the lower molecular weight observed for 50A50E despite similar conversion to other polymers is attributed to the incompatibility of the standard material polystyrene with the polymer containing numerous polar amine functional groups. This results in a relatively higher elution volume. Lastly, the TGA results indicate that none of the polymers exhibited a temperature exceeding 300 °C for 10% decomposition.

Synthesis of CSBO

We prepared soybean oil functionalized with carbonate groups, which can react with the amine pendant groups of the previously synthesized poly(AEMA-*ran*-EMA). Carbonated soybean oil (CSBO) was synthesized as a precursor for the NIPU sample by subjecting epoxidized soybean oil (ESBO) to catalytic conditions. The utilized ESBO was confirmed to possess an average of 4.2 epoxy groups per molecule, as verified by the intensity of the peak at δ = 4.3 ppm (H$_d$, CH in the epoxide group) observed in the ^{1}H NMR spectrum (Fig. S7a†). Carbon dioxide gas was continuously bubbled through the ESBO dissolved in hexadecane under atmospheric pressure. A brownish, viscous liquid was obtained after purification. The resulting substance was subsequently analyzed using ^{1}H NMR. The peak at δ = 4.3 ppm (H$_d$) attributed to the epoxy group dis-
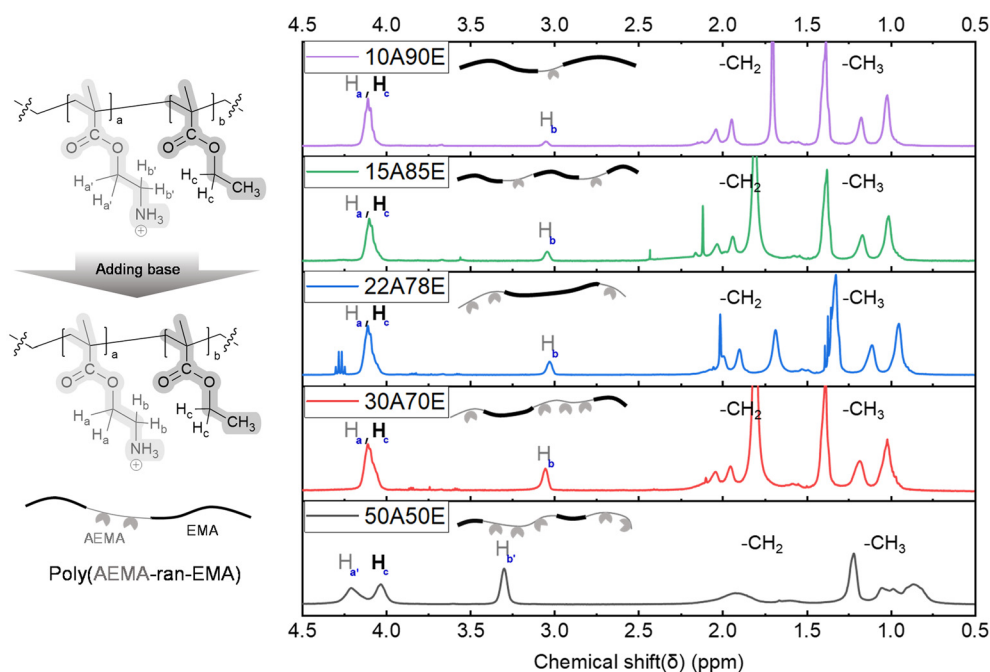
Fig. 2 ^{1}H NMR (400 MHz, D$_2$O) analysis of the synthesized poly(AEMA-*ran*-EMA).

appeared (Fig. S7a†), while a new signal at δ = 4.5–5.2 ppm (H_e, CH in 5CC group) corresponding to the 5CC group emerged[48] (Fig. S7b†). It can be deduced that 91 mol% of the epoxide groups underwent conversion into the 5CC group.

Synthesis of NIPU samples

Following the preparation of well-defined poly(AEMA-*ran*-EMA) and CSBO, five series of soybean oil-based NIPU samples ("Co-NIPU-1" to "Co-NIPU-5") were synthesized using DMSO as the solvent. DMSO offers significant advantages as a solvent in this synthesis due to its exceptional solubilizing power and ability to dissolve a wide range of polymers and reactants. Furthermore, its high boiling point and excellent thermal stability make DMSO a safer and less toxic alternative to traditional organic solvents, while also enabling efficient reactions at elevated temperatures.[49] Importantly, DMSO can be recovered and recycled to reduce waste. This is possible because during solvent casting, only DMSO volatilizes, making it easy to separate from non-volatile substances.

Upon performing a time-dependent analysis of the FT-IR graph using the co-NIPU-5 sample, it was determined that the reaction between the primary amine groups and the 5CC groups stopped advancing from 24 to 48 hours (Fig. S8†). Consequently, a reaction time of 24 hours was adopted in the synthesis approach. The solution was maintained at a temperature of 125 °C without stirring, while maintaining continuous solvent evaporation. After 24 hours, the solvent had completely evaporated, resulting in the formation of a uniform film with a thickness of less than 0.5 mm. For co-NIPU-1, the sample containing the copolymer with the highest F_{EMA} value, a yellowish product was observed. As the F_{EMA} value decreased, the resulting product exhibited a progressively darker brownish color.

Each co-NIPU-*x* series was subjected to Fourier transform infrared spectroscopy (FT-IR) analysis (Fig. 3). All of the samples showed a broad peak at 3000–3500 cm^{-1} (blue area), representing the hydroxyl group formed through carbamate linkage. The three types of carbonyl groups observed in the wavenumber range of 1600–1800 cm^{-1} originate from distinct positions within the molecule: the absorption peak at 1800 cm^{-1} is attributed to the unreacted 5CC group of CSBO (green dotted line); the peak at 1740 cm^{-1} corresponds to the ester group linked to the main chain of the copolymer (blue dotted line); and the peak at 1680 cm^{-1} is associated with the carbamate group formed by the reaction of the two reactants (red dotted line). Therefore, by comparing the intensity of the peaks at 1800 cm^{-1} and 1680 cm^{-1}, the relative degree of conversion can be evaluated. It was confirmed that copolymers with higher F_{EMA} values exhibited greater reactivity. The low reactivity of copolymers with small F_{EMA}, in which amine terminal groups are closely spaced together, supports the prediction that steric hindrance is a significant determining factor. Overall, in contrast to previous observations with PAEMA and CSBO at a 1 : 1 stoichiometric ratio resulting in low conversion (Fig. S5†), the reaction between the random copolymer poly(AEMA-*ran*-EMA) and CSBO at the same ratio exhibited comparatively higher conversion.
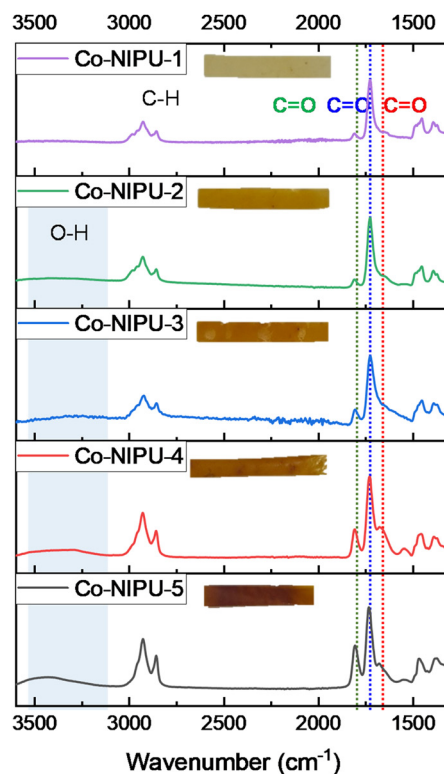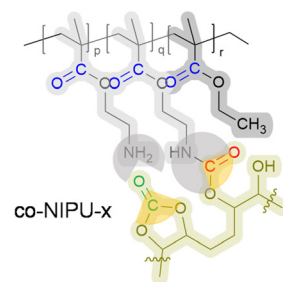

Fig. 3 Fourier-transform infrared (FT-IR) spectra of co-NIPU-*x* samples synthesized using poly(AEMA-*ran*-EMA).

Mechanical properties of co-NIPU-*x*

To examine the mechanical properties of the synthesized co-NIPU-*x* sample, a tensile test was conducted to obtain the Young's modulus (E), tensile strength (σ_R), and elongation at break (ε_R) values (Fig. 4a). Co-NIPU-1 and co-NIPU-2 exhibited greater stiffness and resistance to fracture than others: σ_R > 25 MPa and E > 650 MPa, representing the highest values reported for soybean oil-based NIPU to date[26–32,34,48] (Fig. 4c and Table 2). Additionally, a noticeable decrease in Young's modulus was observed when the F_{EMA} value of the copolymer in the NIPU sample was lower than that of co-NIPU-3. By adjusting the monomer ratio, the Young's modulus spanned over a range greater than 17-fold, and the tensile stress spanned over a range greater than 12-fold. Furthermore, co-NIPU-5 exhibited a higher ε_R value compared with the other NIPU samples. A significant rise in E and a drop in ε_R following the elimination of unreacted CSBO residue from co-NIPU-5
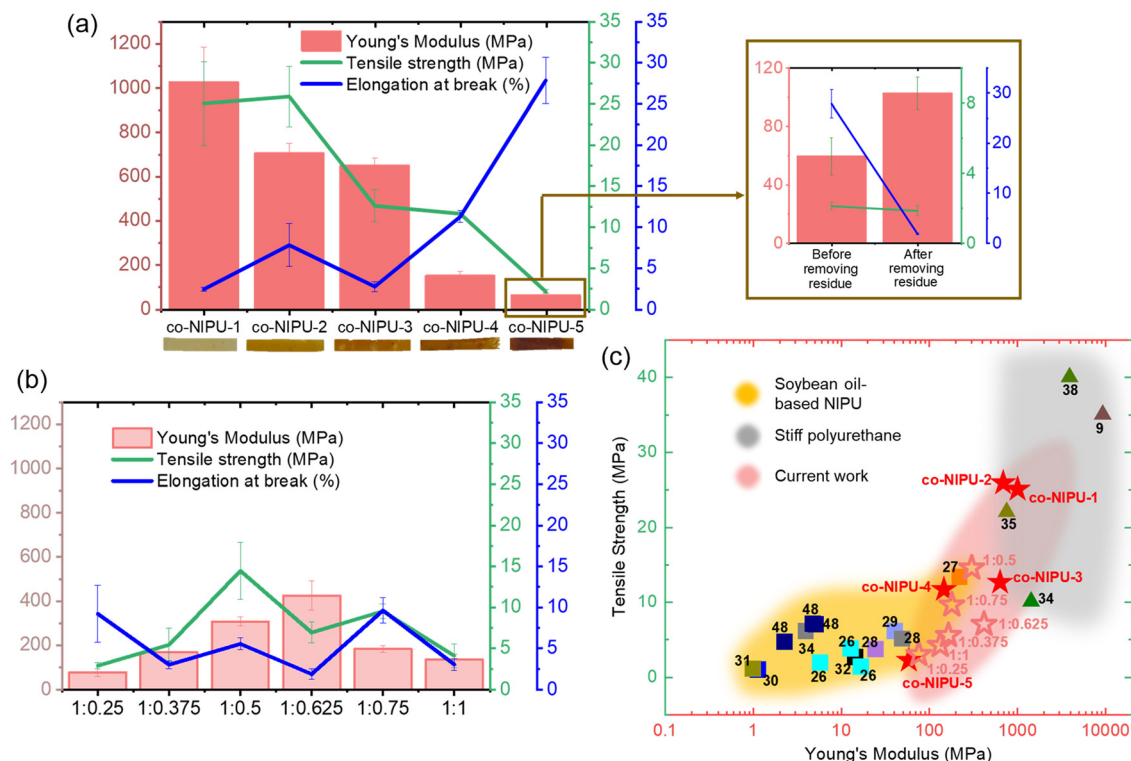
Fig. 4 Characterization of NIPU. Tensile test. (a) The result of co-NIPU-x samples synthesized using poly(AEMA-*ran*-EMA) as a reactant, with additional data of co-NIPU-5 before and after removing CSBO residue using toluene. (b) The result of NIPU samples synthesized using PAEMA as a reactant. (c) Comparison of the mechanical properties of soybean oil-based NIPUs with previous relevant polyurethane research.

Table 2 Mechanical and adhesion properties of synthesized co-NIPU-x series

NIPU sample	co-NIPU-1	co-NIPU-2	co-NIPU-3	co-NIPU-4	co-NIPU-5
Young's modulus, E (MPa)	1030 ± 160	700 ± 50	650 ± 30	150 ± 20	60 ± 10
Tensile strength, σ_R (MPa)	25 ± 5	26 ± 4	13 ± 2	11.6 ± 0.2	2.1 ± 0.2
Elongation at break, ε_R (%)	2.5 ± 0.2	8 ± 3	2.7 ± 0.6	11.2 ± 0.7	28 ± 3
Lap shear strength (MPa)	1.5 ± 0.1	3.8 ± 0.5	7.2 ± 0.4	2.2 ± 0.3	1.7 ± 0.1

using of toluene indicate that the excess unreacted CSBO acts as a plasticizer.

To determine whether the mechanical properties and broad range of performance depend on the proportion of the EMA segment, we conducted experiments on NIPU samples based on polymers composed solely of AEMA and observed lower limits of Young's modulus and tensile strength compared to those based on the copolymer. PAEMA-based samples were synthesized using the same method by adjusting the molar ratios of the primary amine pendant group of the polymer to the 5CC group in CSBO to 1:0.25, 1:0.375, 1:0.5, 1:0.625, 1:0.75, and 1:1 (Fig. 4b). As the input quantity of CSBO increases from 1:0.25 to approximately 1:0.5 ~ 0.625, there is a corresponding increase in both E and σ_R. This suggests that the observed pattern arises from the influence of crosslinking density. However, once the quantity of CSBO surpasses a specific threshold (1:0.625), both E and σ_R exhibit a subsequent decline because of the plasticizing effect of unreacted

CSBO. The utilization of PAEMA, a polymer in which pendant groups provide the highest number of reaction sites, can lead to the formation of unreacted residues when CSBO exceeds a specific quantity due to steric hindrance. The highest E (= 429 MPa) was obtained at a 1:0.625 ratio and the highest σ_R (= 14.5 MPa) was obtained at a 1:0.5 ratio. This still results in softer mechanical properties compared with co-NIPU-1, 2 and 3.

To further investigate the effect of polymer architecture on the mechanical properties of NIPU, additional experiments were conducted using NIPU samples synthesized from poly(AEMA-*block*-EMA). As shown in Fig. S9,† the Young's modulus of the block copolymer-based NIPU remains comparable to that of the homopolymer-based NIPU, indicating that structuring AEMA and EMA into blocks does not significantly enhance mechanical performance. This result can be attributed to the localized concentration of AEMA segments within the block copolymer, which restricts uniform crosslinking with CSBO

and limits the formation of an interconnected network. In contrast, the random copolymer ensures a more homogeneous distribution of AEMA units, leading to efficient crosslinking and improved mechanical properties. These findings emphasize that the random copolymerization of AEMA and EMA is essential for optimizing monomer reactivity and achieving superior mechanical reinforcement in NIPU materials.

The synthesis of samples using three distinct types of amine-terminated polymers demonstrates that the uniform distribution of the EMA segment plays a significant role in influencing the material properties. This observation will be further analyzed in the following sections through powder X-ray diffraction (XRD) and differential scanning calorimetry (DSC) experiments.

X-ray diffraction analysis of co-NIPU-*x*

The structural predictions of co-NIPU-*x* samples are further validated by XRD analysis (Fig. 5). In the case of PEMA, discernible peaks are evident at peak I ($2\theta_{XRD} = 12.0°$) and peak II ($2\theta_{XRD} = 17.8°$). Peak II, which represents relatively narrower spacing, corresponds to the interatomic distance during van der Waals contact,[39] predominantly reflecting the correlation among ethyl groups within the side chain. On the other hand, peak I signifies coherence between polymer strands extending beyond the van der Waals distance, further indicating short-range ordering between different chains.

The most notable aspect in XRD results is that the peak II signal remains in the similar position even after carbamate linkage formation (co-NIPU-1, 2 and 3). However, its intensity decreases with lower F_{EMA} values, ultimately vanishing after the co-NIPU-4 stage. The disappearance of the peak upon the inclusion of a high content of CSBO and AEMA suggests that

the EMA segments are responsible for this peak, and its weakening correlates with an increase in EMA mobility. These findings indicate that in NIPU samples with high F_{EMA} values, short-range ordering within EMA segments is preserved, contributing to stronger intermolecular interactions.

An additional noteworthy observation in the XRD result is that the peak shifts to the left as the F_{EMA} value of the copolymer in the NIPU sample decreases. The increase in intermolecular distance (d_{XRD}) between PEMA strands indicates that a drop in F_{EMA} values leads to greater EMA segment mobility, resulting in softer mechanical properties with lower moduli. This correlation is further supported by mechanical analysis (Fig. 4), where the Young's modulus (E) trends align with XRD peak shifts. Specifically, as d_{XRD} increases due to reduced EMA content, weaker van der Waals interactions lead to decreased stiffness.

This phenomenon can also be verified through the glass transition temperature (T_g) peak obtained by DSC analysis (Fig. S10 and Table S1†). The peak observed around 0–10 °C in co-NIPU-5 is attributed to the phase transition of unreacted CSBO residue. In the synthesis of co-NIPU-*x* using a polymer containing a low EMA component, the T_g peak was not observed, similar to a typical thermoset polymer. Interestingly, however, for co-NIPU-1 and co-NIPU-2, the T_g peak was detected at a position similar to that of the PEMA.[50] The T_g peak of a thermoset polymer with a low crosslinking density can be attributed to the presence of an amorphous region, which is expected for the EMA segment with a linear structure. This interpretation can be confirmed by the positional similarity of the XRD signals in the PEMA polymer and the NIPU sample.

One of the unusual findings is that NIPU samples do not exhibit the peak I signal, unlike PEMA, despite the addition of
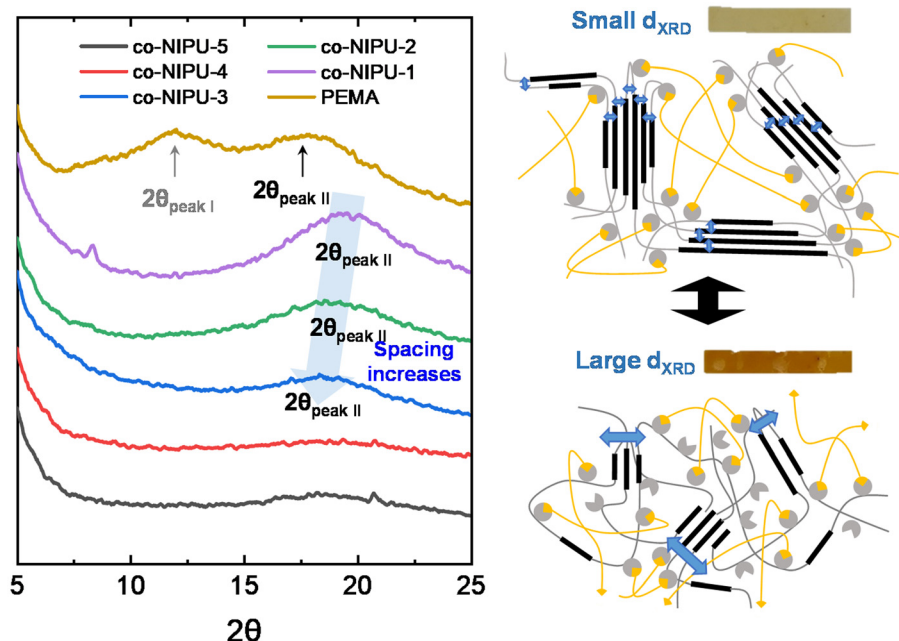

Fig. 5 Characterization of co-NIPU-*x* and PEMA: powder X-ray diffraction (XRD).

a small amount of CSBO. According to the spatially restricted layer structure, peak I can be interpreted as the intersegmental distance between neighbouring side chains. In contrast, Genix *et al.* stated that peak I reflects correlations involving main chain atoms, especially between the main chain and the COO group. As evidenced by the preservation of the peak I signal, it can be concluded that the terminal ethyl group in PEMA solely maintains the short-range order in the bulk, as the CSBO molecule forms carbamate bonds in the sample.

Despite the challenges associated with precisely determining the structure, it can be concluded that the unidirectional shift of the XRD peak is highly related to changes in the EMA segment structure and the overall mechanical properties of the co-NIPU-*x* sample.

Adhesion properties of co-NIPU-*x*

The superior adhesion properties of NIPU, compared to those of the carbamate linkages derived from isocyanates, are attributed to the presence of an additional hydroxyl group on the β-carbon. The presence of hydroxyl groups in the co-NIPU-*x* sample was confirmed through FT-IR analysis (Fig. 3). In particular, samples containing polymers with lower F_{EMA} values exhibited higher intensity.

To validate the adhesion properties of the NIPU samples, lap shear tests were conducted using soda-lime glass as the substrate, given its prevalence in production. The samples were prepared using the same procedure as that used for the synthesis of film-forming co-NIPU-*x*; however, the reaction was temporarily halted when the total volume of the solution in DMSO reached 1.5 mL, and the resulting gel-type material was then applied to the substrate. Subsequently, the remaining solvent was completely evaporated while applying a pressure of 20 kPa using a weight. The lap shear strength of glass-based samples, each incorporating a series of co-NIPU-*x*, was measured using tensile mode testing (Fig. 6a).

The adhesion properties of co-NIPU-*x* are primarily influenced by the presence of carbamate groups, which provide strong cohesive and adhesive energy through hydrogen bonding and dipole interactions. The formation of these carbamate linkages depends on the availability of amine groups from AEMA and their reaction with the 5CC group in CSBO. Co-NIPU-3 exhibits the highest adhesion strength (~7 MPa) because its AEMA-to-EMA ratio ensures sufficient carbamate formation while maintaining an optimal crosslinking density for effective interfacial interactions. In contrast, co-NIPU-5, which has a lower crosslinking density and fewer carbamate linkages relative to the total volume, exhibits weaker adhesion properties. These trends are further supported by FT-IR analysis, which confirms the presence of hydroxyl groups associated with carbamate formation (Fig. 3). The relationship between monomer composition, carbamate formation, and adhesion strength highlights the critical role of the random copolymer architecture in optimizing interfacial bonding strength in NIPU materials.

The lap shear strength of NIPU incorporating ethylenediamine and *m*-xylenediamine was measured and compared for analysis. Unlike co-NIPU-*x*, all monomer-based samples exhibited low values below 1 MPa with cohesive failure. This difference is attributed to the higher cohesive strength exhibited by co-NIPU-*x*. The high cohesive strength of the adhesive layer enhances the tensile strength under mechanical stress.[51] Consequently, among soybean oil-based NIPUs, co-NIPU-*x* exhibits a high modulus and tensile strength (Fig. 4), providing sufficient cohesive energy to withstand stress until adhesion failure occurs.

A comparative analysis with existing soybean oil-based adhesives highlights the significance of polymer architecture and crosslinking chemistry in determining adhesion performance. Soybean oil-derived adhesives have been explored extensively as a sustainable alternative to petroleum-based adhesives, with formulations ranging from citric acid-cross-
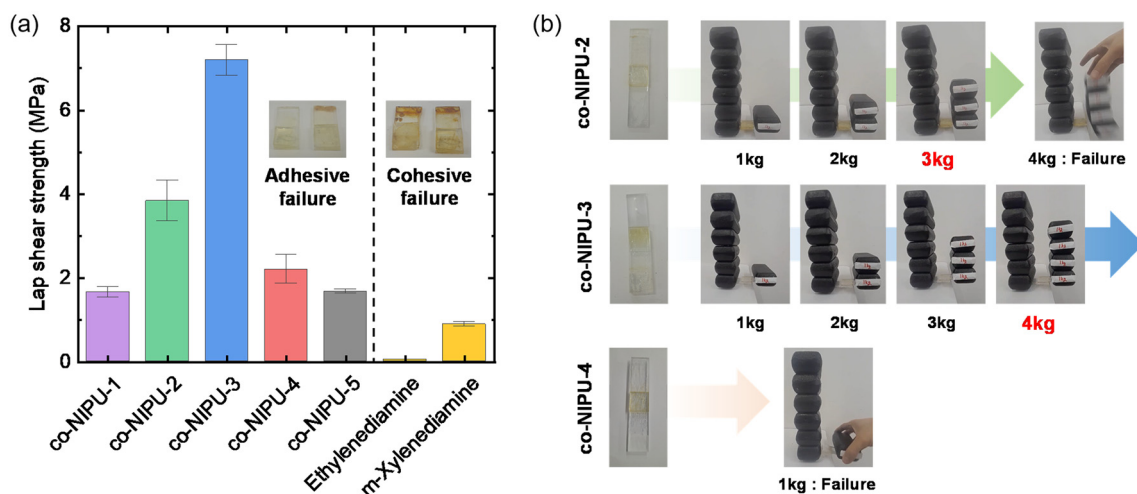

Fig. 6 Characterization of co-NIPU-*x*. Adhesion property test. (a) Shear lap test results for co-NIPU-*x* series and amine monomer-based NIPU. (b) A snapshot illustrating the load-bearing capacity of co-NIPU-2, co-NIPU-3, and co-NIPU-4.

linked networks to polyurethane-based systems. These bio-based adhesives typically leverage the presence of hydroxyl and ester groups to enhance adhesion through hydrogen bonding and network formation. For instance, soybean oil crosslinked with citric acid forms β-hydroxyester linkages that enable stress relaxation and self-healing, though its lap shear strength remains relatively low (~0.65 MPa), limiting its structural applications.[52] Similarly, polyurethane adhesives synthesized from soybean oil-based polyols have demonstrated moderate lap shear strength (~2.0 MPa), with adhesion performance largely dictated by the density of urethane linkages and cross-linking efficiency.[53] Another notable approach involves photo-reversible adhesives utilizing soybean oil as a backbone, where coumarin-functionalized epoxidized soybean oil enables adhesion tunability under UV irradiation. While this system offers reusability advantages, its lap shear strength (~3.1 MPa) remains well below that required for structural bonding applications.[54] Another study reported that soybean oil–urea–formaldehyde (UF) hybrid systems achieved a lap shear strength of approximately 4.5 MPa without plasma treatment.[55]

Despite these advancements, the adhesion performance of co-NIPU-3 (~7 MPa) surpasses those of existing soybean oil-based adhesives, demonstrating the critical role of polymer architecture in optimizing adhesion strength. This distinction underscores the superior performance of co-NIPU materials compared to conventional soybean oil-derived adhesives, making them promising candidates for high-strength, bio-based adhesive applications.

To evaluate practical applicability, co-NIPU-x was applied to a 6.8 cm^2 area on soda-lime glass to determine its load-bearing capacity, with forces exerted perpendicular to the surface (Fig. 6b). Consistent with the overall trend observed in the lap shear test, co-NIPU-3 was observed to withstand a maximum weight of 4 kg.

Chemical resistance of co-NIPU-x

In order to determine the chemical resistance of the co-NIPU-x sample, a swelling test was conducted using two types of solvents: water representing a hydrophilic solvent and toluene representing a hydrophobic solvent (Fig. 7). The swelling ratio
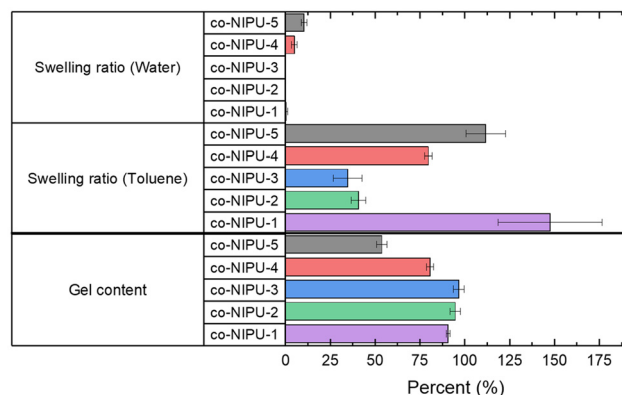
remains relatively low (<10%) for all five in the case of water, whereas a significant trend is observed in toluene, depending on the EMA monomer content. Co-NIPU-1, 2, and 3 exhibit gel contents exceeding 90 percent, while a decrease in the F_{EMA} value of the copolymer correlates with a decrease in gel content to below 60 percent. The swelling ratio of NIPU against toluene typically declines as the F_{EMA} value of the copolymer reactant increases, with the exception of co-NIPU-1, which exhibits a high value of ~150% (Table S1†). Considering that linear PEMA dissolves in some organic solvents, including toluene,[56] the low degree of crosslinking in co-NIPU-1 samples hardly enhances organic solvent resistance. For NIPU samples with low gel content (co-NIPU-4 and 5), the presence of voids in NIPU generated by CSBO residue leads to higher absorption of solvent, resulting in an increase in gel content. Additional confirmation of the presence of unreacted CSBO residue can be obtained from the tensile test results of the CSBO residue-eliminated co-NIPU-5 sample.

Thermal properties of co-NIPU-x

The thermal stability of co-NIPU-x samples was evaluated using thermogravimetric analysis (TGA) (Fig. 8). The first peak at 250–300 °C ($T_{peak\ I}$) and the second peak at 300–400 °C ($T_{peak\ II}$) of PEMA detected in derivative thermogravimetric analysis (DTG) data do not appear within the same temperature range in all co-NIPU-x samples. Each peak corresponds to successive processes of polymethacrylic acid formation ($T_{peak\ I}$)
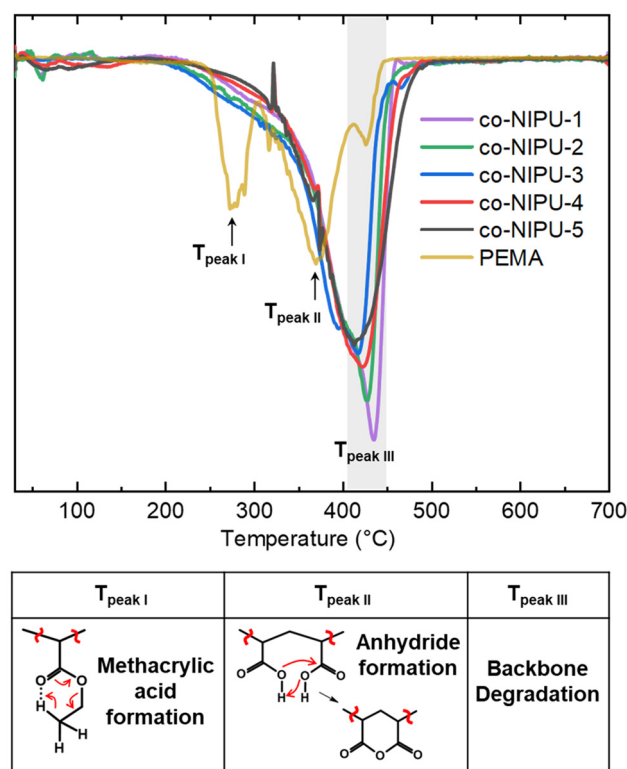

Fig. 7 Characterization of co-NIPU-x: gel content analysis.

Fig. 8 Characterization of co-NIPU-x: thermogravimetric analysis.

and anhydride formation ($T_{peak\ II}$), respectively.[57] It is conjectured that the absence of polymethacrylic acid formation is due to crosslinking, which reduces the mobility of the polymer and thus decreases effective collisions for successive decomposition reactions. The third peak of PEMA at 400–450 °C ($T_{peak\ III}$), which indicates degradation of the polymer backbone, is also detected in co-NIPU-x within the same temperature range but with a greater intensity.[58] Regarding the TGA results for the linear copolymer (Table 1), additional crosslinking with CSBO improves the thermal stability of the polymer. Moreover, an adverse correlation is noted between $T_{peak\ III}$ and the content of CSBO in co-NIPU-x synthesis (Table S1†). This phenomenon may be due to the fact that CSBO exhibits a lower DTG peak temperature than that of the copolymer backbone, leading to an overall reduction in the observed $T_{peak\ III}$ with increasing CSBO content.[59]

Conclusion

By successfully developing a stiff NIPU using soybean oil, this study expands the potential of bio-based materials in applications traditionally dominated by petroleum-derived stiff polyurethanes, contributing to the advancement of green polymer chemistry. Our group enhanced both Young's modulus and tensile strength, surpassing those of previously reported soybean oil-based NIPUs. This enhancement is attributed to the copolymers with higher EMA content, which displayed short-range ordered structures, as corroborated by XRD and DSC analyses. The flexibility in adjusting the copolymer composition allows for the continuous and deliberate modification of NIPU properties, paving the way for the synthesis of customized, high-performance materials suitable for a wide range of industrial applications.

The versatility of co-NIPU-x is further supported by the enhanced adhesion properties, thermal stability, and chemical resistance analysis. The higher lap shear strength observed in co-NIPU-x, particularly co-NIPU-3, is attributed to its higher cohesive strength compared to monomer-based NIPU samples. The thermal stability test demonstrated that the co-NIPU-x samples could withstand high temperatures while maintaining their structural integrity. Additionally, the chemical resistance test revealed that while the NIPU samples showed varying swelling ratios in toluene, co-NIPU-3 exhibited the lowest swelling ratio, indicating its superior robustness in chemical environments.

This work highlights the feasibility of utilizing soy-based feedstocks to create high-performance polyurethane materials. The presented approach demonstrates that unlike conventional stiff polyurethanes, which primarily rely on petroleum-derived precursors, soybean oil-based NIPUs can achieve enhanced mechanical properties while maintaining sustainability advantages. This advancement expands the applicability of soy-based polymers to industries traditionally dependent on high-load-bearing materials, such as structural composites, adhesives, and protective coatings.

Data availability

All relevant data are included within the manuscript and its ESI.†

Conflicts of interest

There are no conflicts to declare.

Acknowledgements

References

1 T. Engels, in *Thermosets*, Elsevier, 2018, pp. 341–368.
2 F. M. de Souza, J. Choi, T. Ingsel and R. K. Gupta, in *Nanotechnology in the Automotive Industry*, Elsevier, 2022, pp. 105–129.
3 A. Kausar, *Am. J. Polym. Sci. Eng.*, 2017, **5**, 1–12.
4 L. Xu, X. Li, F. Jiang, X. Yu, J. Wang and F. Xiao, *Constr. Build. Mater.*, 2022, **344**, 128252.
5 T. Engels, in *Thermosets*, Elsevier, 2018, pp. 228–253.
6 H. Wu, M. Yang, W. Song, Z. Wu, D. Chen and X. Chen, *Constr. Build. Mater.*, 2024, **411**, 134798.
7 A. Cornille, R. Auvergne, O. Figovsky, B. Boutevin and S. Caillol, *Eur. Polym. J.*, 2017, **87**, 535–552.
8 C. Zhang, H. Wang and Q. Zhou, *Green Chem.*, 2020, **22**, 1329–1337.
9 B. Pössel and R. Mülhaupt, *Macromol. Mater. Eng.*, 2020, **305**, 2000217.
10 S. El Khezraji, H. Ben Youcef, L. Belachemi, M. A. Lopez Manchado, R. Verdejo and M. Lahcini, *Polymers*, 2023, **15**, 254.
11 B. Rangarajan, A. Havey, E. A. Grulke and P. D. Culnan, *J. Am. Oil Chem. Soc.*, 1995, **72**, 1161–1169.
12 T. Saurabh, M. Patnaik, S. Bhagt and V. Renge, *Int. J. Adv. Eng. Technol.*, 2011, **2**, 491–501.
13 U. S. D. o. Agriculture, Crop Explorer for Major Crop Regions, **https://apps.fas.usda.gov/psdonline/circulars/oilseeds.pdf**, (accessed 21 Feb, 2024).

14 A. D'Amato, S. Paleari, M. Pohjakallio, I. Vanderreydt and R. Zoboli, *Plastics Waste Trade and the Environment*, ETC/WMGE, Copenhagen, 2019.

15 D. Simón, A. Borreguero, A. De Lucas and J. Rodríguez, *Waste Manage.*, 2018, **76**, 147–171.

16 I. Javni, D. P. Hong and Z. S. Petrović, *J. Appl. Polym. Sci.*, 2008, **108**, 3867–3875.

17 S. Matsumura, Y. Soeda and K. Toshima, *Appl. Microbiol. Biotechnol.*, 2006, **70**, 12–20.

18 E. Vangronsveld, S. Berckmans and M. Spence, *Ann. Occup. Hyg.*, 2013, **57**, 650–661.

19 G. Rokicki and A. Piotrowska, *Polymer*, 2002, **43**, 2927–2935.

20 H. Khatoon, S. Iqbal, M. Irfan, A. Darda and N. K. Rawat, *Prog. Org. Coat.*, 2021, **154**, 106124.

21 E. K. Leitsch, W. H. Heath and J. M. Torkelson, *Int. J. Adhes. Adhes.*, 2016, **64**, 1–8.

22 P. Zhang, B. Zhang, J. Pan, G. Zhang, C. Ma and G. Zhang, *Chem. Mater.*, 2023, **35**, 7730–7740.

23 C. Bakkali-Hassani, D. Berne, P. Bron, L. Irusta, H. Sardon, V. Ladmiral and S. Caillol, *Polym. Chem.*, 2023, **14**, 3610–3620.

24 G. Beniah, D. J. Fortman, W. H. Heath, W. R. Dichtel and J. M. Torkelson, *Macromolecules*, 2017, **50**, 4425–4434.

25 N. S. Purwanto, Y. Chen and J. M. Torkelson, *ACS Appl. Polym. Mater.*, 2023, **5**, 6651–6661.

26 S. Samanta, S. Selvakumar, J. Bahr, D. S. Wickramaratne, M. Sibi and B. J. Chisholm, *ACS Sustainable Chem. Eng.*, 2016, **4**, 6551–6561.

27 L. Poussard, J. Mariage, B. Grignard, C. Detrembleur, C. Jérôme, C. Calberg, B. Heinrichs, J. De Winter, P. Gerbaux and J.-M. Raquez, *Macromolecules*, 2016, **49**, 2162–2171.

28 O. Lamarzelle, P.-L. Durand, A.-L. Wirotius, G. Chollet, E. Grau and H. Cramail, *Polym. Chem.*, 2016, **7**, 1439–1451.

29 H. Gholami and H. Yeganeh, *Eur. Polym. J.*, 2021, **142**, 110142.

30 G. Caballero-García and J. M. Goodman, *Org. Biomol. Chem.*, 2021, **19**, 9565–9618.

31 J. Li, X. Lin, X. Yang, X. Xu, H. Liu and M. Zuo, *Ind. Crops Prod.*, 2023, **200**, 116842.

32 X. Yang, S. Wang, X. Liu, Z. Huang, X. Huang, X. Xu, H. Liu, D. Wang and S. Shang, *Green Chem.*, 2021, **23**, 6349–6355.

33 P. Somdee, M. A. Ansari and K. Marossy, *Polym. Compos.*, 2023, **44**, 401–412.

34 M. Bähr and R. Mülhaupt, *Green Chem.*, 2012, **14**, 483–489.

35 H. Blattmann and R. Mülhaupt, *Macromolecules*, 2016, **49**, 742–751.

36 P. Patel, F. M. de Souza and R. K. Gupta, *ACS Omega*, 2024, **9**, 5862–5875.

37 S. Jalilian and H. Yeganeh, *Polym. Bull.*, 2015, **72**, 1379–1392.

38 M. Szycher, *Szycher's Handbook of Polyurethanes*, CRC Press, Boca Raton, Florida, 2nd edn, 2012.

39 R. L. Miller, R. F. Boyer and J. Heijboer, *J. Polym. Sci., Polym. Phys. Ed.*, 1984, **22**, 2021–2041.

40 M. Wind, R. Graf, S. Renker, H. W. Spiess and W. Steffen, *J. Chem. Phys.*, 2005, **122**, 014906.

41 J. T. Lai, D. Filla and R. Shea, *Macromolecules*, 2002, **35**, 6754–6756.

42 S. J. Park, F. L. Jin and J. R. Lee, *Macromol. Rapid Commun.*, 2004, **25**, 724–727.

43 H. Jianying, C. Jiayan, Z. Jiaming, C. Yihong, D. Lizong and Z. Yousi, *J. Appl. Polym. Sci.*, 2006, **100**, 3531–3535.

44 S.-E. Dechent, A. W. Kleij and G. A. Luinstra, *Green Chem.*, 2020, **22**, 969–978.

45 M. R. Aguilar, A. Gallardo, M. D. M. Fernández and J. S. Román, *Macromolecules*, 2002, **35**, 2036–2041.

46 C. Zheng, *Soft Matter*, 2019, **15**, 5357–5370.

47 T. Tiainen, J. K. Mannisto, H. Tenhu and S. Hietala, *Langmuir*, 2021, **38**, 5197–5208.

48 Z. Li, Y. Zhao, S. Yan, X. Wang, M. Kang, J. Wang and H. Xiang, *Catal. Lett.*, 2008, **123**, 246–251.

49 M. Marti, L. Molina, C. Aleman and E. Armelin, *ACS Sustainable Chem. Eng.*, 2013, **1**, 1609–1618.

50 P. D. Condo and K. P. Johnston, *J. Polym. Sci., Part B: Polym. Phys.*, 1994, **32**, 523–533.

51 J. Klingen, *Adhesive Bonding in Five Steps: Achieving Safe and High-Quality Bonds*, John Wiley & Sons, 2022.

52 F. I. Altuna, V. Pettarin and R. J. Williams, *Green Chem.*, 2013, **15**, 3360–3366.

53 U. Panchal, M. L. Chaudhary, P. Patel, J. Patel and R. K. Gupta, *ACS Omega*, 2024, **9**, 10738–10747.

54 K. Boga, A. F. Patti, J. C. Warner, G. P. Simon and K. Saito, *ACS Appl. Polym. Mater.*, 2023, **5**, 4644–4653.

55 Z. Duan, M. Hu, S. Jiang, G. Du, X. Zhou and T. Li, *ACS Sustainable Chem. Eng.*, 2022, **10**, 3363–3372.

56 K. Kaur, A. R. Iyer, S. W. Campbell and V. R. Bhethanabotla, *J. Chem. Eng. Data*, 2020, **65**, 5046–5054.

57 J. Cervantes-Uc, J. Cauich-Rodríguez, H. Vázquez-Torres and A. Licea-Claveríe, *Polym. Degrad. Stab.*, 2006, **91**, 3312–3321.

58 R. Benlikaya, M. Alkan and İ. Kaya, *Polym. Compos.*, 2009, **30**, 1585–1594.

59 P. Chand, C. V. Reddy, J. G. Verkade, T. Wang and D. Grewell, *Energy Fuels*, 2009, **23**, 989–992.